Nanoscale Advances

PAPER

View Article Online
View Journal | View Issue

Open Access Article. Published on 03 Desember 2018. Downloaded on 15/03/2026 14.09.46.
This article is licensed under a Creative Commons Attribution-NonCommercial 3.0 Unported Licence.

Check for updates

Cite this: *Nanoscale Adv.*, 2019, **1**, 189

# Photocatalytic overall water splitting on Pt nanocluster-intercalated, restacked $KCa_2Nb_3O_{10}$ nanosheets: the promotional effect of co-existing ions†

Takayoshi Oshima,[ab] Yunan Wang,[c] Daling Lu,[d] Toshiyuki Yokoi[c] and Kazuhiko Maeda *[a]

Received 25th September 2018
Accepted 3rd December 2018

DOI: 10.1039/c8na00240a

rsc.li/nanoscale-advances

Promotional effects of co-existing ions on overall water splitting into $H_2$ and $O_2$ have been studied in bulk-type semiconductor photocatalysts (*e.g.*, $TiO_2$), but such an effect remains unexplored in two-dimensional nanosheet photocatalysts. Here we examined the effect of co-existing ions on the photocatalytic water splitting activity of Pt nanocluster-intercalated $KCa_2Nb_3O_{10}$ nanosheets. Interestingly, not only anions, as usually observed in bulk-type photocatalysts, but also cations had a significant influence on the photocatalytic performance. The rates of $H_2$ and $O_2$ evolution over Pt/$KCa_2Nb_3O_{10}$ as well as the product stoichiometry were improved in the presence of NaI. $I^-$ ions were found to effectively suppress undesirable backward reactions, consistent with the previous work by Abe *et al.* (*Chem. Phys. Lett.*, 2003, **371**, 360–364). On the other hand, $Na^+$ ions in the reaction solution were exchanged for $K^+$ in the interlayer space of $KCa_2Nb_3O_{10}$ during the water splitting reaction, which promoted interlayer hydration and consequently improved photocatalytic performance.

## Introduction

Clean production of hydrogen by water splitting over a semiconductor photocatalyst has attracted considerable interest in order to meet the social demand for replacing $CO_2$-emitting fossil fuels with clean energy sources.[1–3] The efficiency of photocatalytic water splitting, however, still remains unsatisfactory. Therefore, not only enhancing the performance of known photocatalysts but also fundamental investigation, for example understanding the reaction mechanism and exploring new materials, is important in this research field.

Certain layered materials undergo exfoliation, producing colloidal suspensions of unilamellar sheets.[4–27] The planar size of the exfoliated sheets typically ranges from several hundreds of nanometers to a few micrometers, with a thickness of 1–2 nm. Because of the sheet-like two-dimensional (2D) structure, it is called a nanosheet. The nanosheets containing certain transition metal cations such as $Ti^{4+}$, $Nb^{5+}$, $Ta^{5+}$, and $W^{6+}$ are known to exhibit photocatalytic activity. They are expected to have several advantages in heterogeneous photocatalysis, compared with conventional bulk-type 3D photocatalysts (*e.g.*, $TiO_2$).

It is known that high crystallinity of a semiconductor has a positive impact on photocatalytic performance for overall water splitting, because of the prolonged lifetime of photogenerated electrons and holes.[28] To obtain a highly crystalline material, high calcination temperature is generally required in the synthesis process; however, such harsh calcination conditions facilitate grain growth of photocatalyst particles, resulting in smaller surface area and lower density of reaction sites, and *vice versa*.[29] Moreover, larger size of semiconductor particles can have a negative effect in terms of carrier diffusion to the surface, resulting in recombination between electrons and holes and lowering photocatalytic activity. On the other hand, a nanosheet has both high crystallinity and high surface area owing to its single-crystalline character and anisotropic structure.[30] Furthermore, the small thickness of the nanosheet is expected to shorten the migration distance of photogenerated carriers to the surface, thereby reducing the recombination probability.[9,12] Despite these fascinating features, there are a limited number of examples of overall water splitting using a nanosheet photocatalyst.

Other than such structural factors, there are some key factors to achieve high photocatalytic performance. One of them is

[a]*Department of Chemistry, School of Science, Tokyo Institute of Technology, 2-12-1-NE-2, Ookayama, Meguro-ku, Tokyo 152-8550, Japan. E-mail: maedak@chem.titech.ac.jp*

[b]*Japan Society for the Promotion of Science, Kojimachi Business Center Building, 5-3-1, Kojimachi, Chiyoda-ku, Tokyo 102-0083, Japan*

[c]*Nanospace Catalysis Unit, Institute of Innovative Research, Tokyo Institute of Technology, 4259-S2-5, Nagatsuta, Midori-ku, Yokohama 226-8503, Japan*

[d]*Center for Advanced Materials Analysis, Tokyo Institute of Technology, 4259-R1-34, Nagatsuta-cho, Midori-ku, Yokohama 226-850, Japan*

† Electronic supplementary information (ESI) available. See DOI: 10.1039/c8na00240a

Open Access Article. Published on 03 Desember 2018. Downloaded on 15/03/2026 14.09.46.
This article is licensed under a Creative Commons Attribution-NonCommercial 3.0 Unported Licence.

deposition of metal or metal oxide nanoparticles, which are called co-catalysts, on the photocatalyst surface.[1,2] The loaded co-catalyst serves as active reaction sites and as a promoter for charge separation between electrons and holes, leading to drastic enhancement in photocatalytic performance.[2]

Another one is the reaction conditions, such as co-existing ions and pH.[31–37] For example, Pt-loaded anatase $TiO_2$ achieved overall water splitting into $H_2$ and $O_2$ in the presence of highly concentrated $HCO_3^-$ and/or $CO_3^{2-}$ under basic conditions (pH = 8–11.5)[31] or in a diluted aqueous NaI solution.[32] In these reports, the co-existing anions interacted with Pt, resulting in enhancement of water splitting performance. While effects of reaction conditions on activity have been studied mainly in bulk-type 3D photocatalysts, the photocatalytic activity of nanosheets for overall water splitting has not been investigated enough with respect to reaction conditions.

Recently, we have demonstrated overall water splitting using Pt nanocluster-intercalated, restacked $KCa_2Nb_3O_{10}$ nanosheets.[23,25] In this system, nanosized Pt particles (≤1 nm) were deposited not only on the external surface of $KCa_2Nb_3O_{10}$ but also in the interlayer of the restacked nanosheets. The Pt-intercalated photocatalyst exhibited higher performance compared to the previously reported $RuO_2/KCa_2Nb_3O_{10}$ nanosheets and $Pt/KCa_2Nb_3O_{10}$, the latter of which consisted of Pt nanoparticles deposited only on the external surface of restacked $KCa_2Nb_3O_{10}$ nanosheets.[23] The unprecedented small size of intercalated Pt appears to be responsible for the high performance of this photocatalytic system.

Here we examine, in detail, the photocatalytic water splitting activity of $Pt/KCa_2Nb_3O_{10}$ nanosheets with respect to co-existing ions in reaction solution. The unique photocatalytic properties of the 2D nanosheet material are highlighted for the first time.

## Experimental

### Materials

A $Ca_2Nb_3O_{10}^-$ nanosheet suspension stabilized by tetra(*n*-butyl) ammonium cations ($TBA^+$) was prepared according to a previous report.[9] First, a layered metal oxide, $KCa_2Nb_3O_{10}$, was prepared by solid state reaction by heating a mixture of $K_2CO_3$ (≥99.5%, Kanto Chemical Co.), $CaCO_3$ (≥99.5%, Kanto Chemical Co.), and $Nb_2O_5$ (≥99.95%, Kanto Chemical Co.) in air at 1123 K for 1 h, followed by a second calcination at 1423 K for 10 h in a furnace. The ratio of K, Ca and Nb in the starting mixture was 1.1 : 2 : 3, where 10% excess K was added to compensate for the loss during calcination as reported previously.[9] The resulting $KCa_2Nb_3O_{10}$ was subjected to stirring in $HNO_3$ (60–61%, Wako Pure Chemicals) solution (1 M) for 3 days to exchange $K^+$ in the interlayer for $H^+$. The resulting solid was collected by centrifugation and washed with water repeatedly until the pH of the supernatant became neutral. After the $HCa_2Nb_3O_{10}$ was dried in an oven at 343 K, it was suspended in an aqueous $TBA^+OH^-$ solution (Aldrich Chemical Co., 40 wt% in $H_2O$), followed by stirring for 1 week, yielding a colloidal $TBA^+/Ca_2Nb_3O_{10}^-$ nanosheet suspension. The molar ratio of $TBA^+OH^-$ to exchangeable cations in the layered solids was 1.0.

Pt was deposited on the $KCa_2Nb_3O_{10}$ restacked nanosheets in the same manner as our previous reports.[23,25] An aqueous $[Pt(NH_3)_4]Cl_2$ (Wako Pure Chemicals) solution (1 mM) was added dropwise into the nanosheet suspension containing 5 g of $Ca_2Nb_3O_{10}^-$ nanosheets per L, and the resulting suspension was stirred for one day to adsorb the Pt precursor on the nanosheets. Then, an aqueous KOH (≥86.0%, Kanto Chemical Co.) solution was added to the nanosheet suspension to restack nanosheets, followed by thorough washing with $H_2O$ and drying in an oven. The dried solid was ground into powder with a mortar and a pestle, and heated at 473 K for 1 h under $H_2$ flow (20 mL $min^{-1}$) to obtain $Pt/KCa_2Nb_3O_{10}$ restacked nanosheets.

Adsorption isotherms of NaI on bare $KCa_2Nb_3O_{10}$ or $NaCa_2Nb_3O_{10}$ restacked nanosheets were measured as follows. Typically, 20 mg of sample was dispersed in an aqueous NaI solution with different concentrations (10 mL) and kept at least for one day to achieve adsorption and desorption equilibrium. The resulting suspension was filtered and the filtrate was analyzed by UV-visible absorption spectroscopy (V-565, Jasco). The adsorbed amount of NaI was quantified by a reduction of absorbance at 226.5 nm.

### Characterization

X-ray diffraction (XRD) patterns were recorded on a Rigaku MiniFlex600 powder diffractometer employing monochromatic Cu Kα radiation and operating at 15 mA and 40 kV. Transmission electron microscopy (TEM) images were acquired using a JEM-2010F electron microscope (Jeol). X-ray photoelectron spectra (XPS) were acquired using an ESCA-3400 X-ray photoelectron spectrometer (Shimadzu). The binding energies determined using XPS were corrected with reference to the C 1s peak (284.6 eV) for each sample. $N_2$ adsorption isotherms were measured using a BELSORP-mini instrument (MicrotracBEL) at liquid nitrogen temperature. $H_2O$ adsorption isotherms were acquired at 298 K using a BELSORP-max (MicrotracBEL) instrument. Samples were heated at 473 K for 1 h under vacuum prior to the measurements for both $N_2$ and $H_2O$ adsorption isotherms.

### Photocatalytic reaction

Photocatalytic reactions were performed in an air-free, glass, closed circulation system. A top-irradiation type reaction cell made of Pyrex glass was used, combined with a cooling water bath to maintain the temperature of the reactor at approximately 293 K throughout the reaction. In each reaction, a 50 mg quantity of the restacked nanosheets was suspended in an aqueous solution (100 mL) containing various salts [NaI (≥99.5%, Kanto Chemical Co.), KI (≥99.5%, Kanto Chemical Co.), $Na_2SO_4$ (≥99.0%, Kanto Chemical Co.), or $K_2SO_4$ (≥99.0%, Kanto Chemical Co.)]. After degassing the reaction cell, a small amount (*ca.* 3 kPa) of argon gas was introduced and the suspension was irradiated using a 300 W xenon lamp ($\lambda \geq 300$ nm) to photoexcite $KCa_2Nb_3O_{10}$ that has a band gap of *ca.* 3.6 eV. The light intensity at 350 nm was approximately $1.1 \times 10^{-3}$ einstein per h. The evolved gases were analyzed by gas chromatography (Shimadzu, GC-8A with a TCD detector and an MS-5A column, argon carrier gas).

 This journal is © The Royal Society of Chemistry 2019

Open Access Article. Published on 03 Desember 2018. Downloaded on 15/03/2026 14.09.46.
This article is licensed under a Creative Commons Attribution-NonCommercial 3.0 Unported Licence.

## Results and discussion

### Photocatalytic performance of Pt/$KCa_2Nb_3O_{10}$ for overall water splitting in the presence of various salts

Fig. 1 shows the TEM images of $KCa_2Nb_3O_{10}$ restacked nanosheets with deposited Pt. Very small Pt nanoparticles with homogeneous dispersion were observed on the restacked nanosheets as dark spots due to a difference in electron density between Pt and $KCa_2Nb_3O_{10}$. Our previous study revealed that the deposited Pt was intercalated in the $KCa_2Nb_3O_{10}$ restacked nanosheets with an average size of smaller than 1 nm.[23,24] The details of the structural characterization of the Pt-intercalated $KCa_2Nb_3O_{10}$ nanosheets can be found elsewhere.[23]

Photocatalytic reactions were performed using the Pt/$KCa_2Nb_3O_{10}$ restacked nanosheets in the presence of various salts. Table 1 summarizes the amounts of $H_2$ and $O_2$ evolved in the reaction after 10 h irradiation. When the reaction was carried out in the absence of salts (*i.e.* pure water), a certain amount of $H_2$ was evolved, with a low level of $O_2$ that was far below the stoichiometric value ($H_2/O_2 < 2$). On the other hand, addition of NaI to pure water dramatically improved the photocatalytic performance in terms of both gas evolution amount and $H_2/O_2$ stoichiometry. The experimental error in gas evolution rate was approximately 15%. Neither deactivation nor decomposition of Pt/$KCa_2Nb_3O_{10}$ has been confirmed by XRD and TEM after 30 h irradiation.[23]

In order to investigate in detail the roles of $Na^+$ and $I^-$ in promoting the overall water splitting, KI, $Na_2SO_4$ or $K_2SO_4$ was dissolved in the reaction solution, and photocatalytic activity was examined. The addition of KI to the reaction solution improved the $H_2/O_2$ evolution rates and the stoichiometry, compared to the pure water case, but not as much as that with the addition of NaI. The photocatalytic activity in the presence of $K_2SO_4$ was almost the same as that in pure water, suggesting that both $K^+$ and $SO_4^{2-}$ had little impact on photocatalytic performance. On the other hand, the co-existence of $Na_2SO_4$ in the reaction solution enhanced the performance, although the extent was lower than that observed in the presence of NaI. These results indicate that both $Na^+$ and $I^-$ have a positive influence on the photocatalytic performance of Pt/$KCa_2Nb_3O_{10}$.

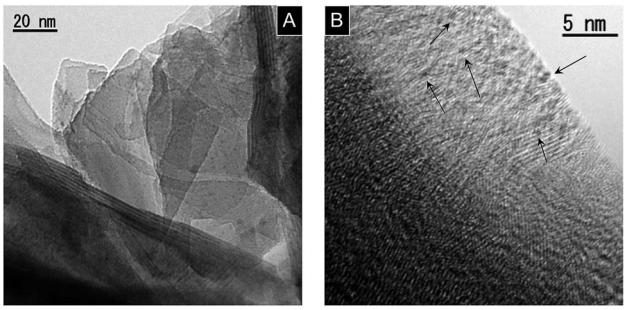


Fig. 1 TEM images of 1.0 wt% Pt/$KCa_2Nb_3O_{10}$ restacked nanosheets. (A) Lower and (B) higher magnification images. Arrows in (B) indicate some deposited Pt nanoclusters.

Table 1 Evolved amounts of $H_2$ and $O_2$ over Pt/$KCa_2Nb_3O_{10}$ restacked nanosheets in various reaction solutions[a]

| Dissolved salt | Amount of evolved gases/μmol | | $H_2/O_2$ ratio |
|---|---|---|---|
| | $H_2$ | $O_2$ | |
| Pure water | 21.6 | 3.6 | 6.0 |
| NaI, 10 mM | 85.5 | 37.4 | 2.3 |
| KI, 10 mM | 33.3 | 12.0 | 2.8 |
| $K_2SO_4$, 5 mM | 20.5 | 2.2 | 9.3 |
| $Na_2SO_4$, 5 mM | 56.4 | 20.0 | 2.8 |

[a] Reaction conditions: catalyst, 50 mg; reaction solution, 100 mL; light source, a 300 W Xe lamp ($\lambda \geq 300$ nm). Reaction time: 10 h.

### Effect of $I^-$

A clear difference was also observed in the time course of overall water splitting in the presence of $I^-$ anions. Fig. 2 shows the time courses of $H_2$ and $O_2$ evolution in an aqueous $Na_2SO_4$ or NaI solution. In the case of $Na_2SO_4$, rates of $H_2$ and $O_2$ evolution gradually decelerated over reaction time, although the initial evolution rates were almost the same as those recorded in the case of NaI, suggesting that backward reaction proceeded as the evolved $H_2$ and $O_2$ were accumulated in the reaction system. On the other hand, the gas evolution rates remained unchanged in the presence of NaI. Moreover, the stoichiometry of evolved $H_2$ and $O_2$ was also improved by NaI addition ($H_2/O_2 \approx 2.3$ for NaI, and 2.8 for $Na_2SO_4$). We observed a similar trend when photocatalytic reactions were performed in aqueous $K_2SO_4$ and KI solution (Fig. S1†). These results suggest that the undesirable reaction (*e.g.*, $H_2/O_2$ recombination and $O_2$ photoreduction) was suppressed in the presence of $I^-$.

Abe *et al.* reported that Pt-loaded $TiO_2$ exhibited much higher water splitting performance in the presence of $I^-$, because the iodine layer formed on Pt nanoparticles could suppress the backward reaction.[32] We also confirmed the effect of $I^-$ on backward reaction in this study. A certain amount of $H_2$

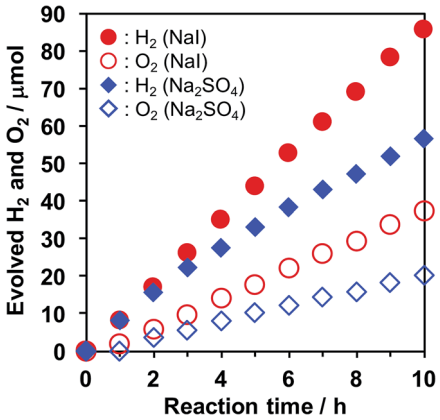


Fig. 2 Time courses of $H_2$ and $O_2$ evolution over Pt/$KCa_2Nb_3O_{10}$ in aqueous solution containing NaI (10 mM, red marks) or $Na_2SO_4$ (5 mM, blue marks). Closed marks: $H_2$; open marks: $O_2$. Reaction conditions: catalyst, 50 mg; reaction solution, 100 mL; light source, a 300 W Xe lamp ($\lambda \geq 300$ nm).

Open Access Article. Published on 03 Desember 2018. Downloaded on 15/03/2026 14.09.46.
This article is licensed under a Creative Commons Attribution-NonCommercial 3.0 Unported Licence.

and $O_2$ was introduced in a closed reaction system and the amount was monitored under dark conditions, as shown in Fig. 3. Although the backward reaction over bare $KCa_2Nb_3O_{10}$ was negligible in pure water, a decrease of $H_2$ and $O_2$ was observed over Pt/$KCa_2Nb_3O_{10}$, indicating that the backward reaction took place on Pt. The water formation rate over Pt/$KCa_2Nb_3O_{10}$ became slower in the presence of NaI than in pure $H_2O$. On the other hand, the backward reaction rate in aqueous $Na_2SO_4$ solution was almost the same as that in pure water. These results suggest that the $I^-$, not $Na^+$, interacted with Pt and suppressed the backward reactions, which are most likely to occur on the externally deposited Pt, contributing to higher photocatalytic activity. Note here that $SO_4^{2-}$ is in principle unreactive during the photocatalytic reaction.[35]

We attempted to detect the iodine species adsorbed on Pt/$KCa_2Nb_3O_{10}$ after the water splitting reaction. However, no iodine signal was observed in this sample (Fig. S2†), most likely because $I^-$ cannot interact with the intercalated Pt due to electrostatic repulsion between negatively charged nanosheets and $I^-$. On the other hand, a small, but distinct photoelectron signal attributable to I 3d was detected in the restacked $KCa_2Nb_3O_{10}$ nanosheets that consisted of externally deposited Pt nanoparticles. It in turn indicates that the number of externally deposited Pt nanoparticles in the present Pt/$KCa_2Nb_3O_{10}$ was not large enough to produce an observable quantity of iodine layers by XPS. Nevertheless, backward reactions that occurred on such lower density Pt islands are significant, and the suppression of the backward reactions is essential. In the photocatalytic reaction, $I^-$ also improved the $H_2/O_2$ stoichiometry. It is known that photo-reduction of $O_2$ proceeds very efficiently on Pt nanoparticles, reducing the $O_2$ evolution performance.[38] Therefore, the improved stoichiometry would originate from the suppression of $O_2$ photo-reduction on Pt as well.

$I^-$ is often used as an electron mediator between $H_2$ and $O_2$ evolution photocatalysts in Z-scheme water splitting.[33,38–41] One may suspect that $I^-$ has a negative impact on photocatalytic performance because the oxidation of $I^-$ on the semiconductor surface hinders water oxidation, which has been observed in Pt/$TiO_2$ at high concentration of NaI.[32] Thus, we investigated the dependence of water splitting performance of Pt/$KCa_2Nb_3O_{10}$ on the NaI concentration. Fig. 4 displays a relationship between $H_2/O_2$ evolution rates in the water splitting reaction and NaI concentration. $H_2$ and $O_2$ evolution rates monotonically increased up to 10 mM NaI and reached a plateau at higher concentration of NaI. UV-visible absorption spectroscopy indicated that before and after the photocatalytic reaction in 10 mM NaI solution, the concentration of $I^-$ remained almost unchanged. These facts indicate that the oxidation of $H_2O$, not $I^-$, dominated on $KCa_2Nb_3O_{10}$. Adsorption isotherm measurement of NaI revealed that no adsorption of $I^-$ took place on the surface of bare $KCa_2Nb_3O_{10}$. The surface properties inhibited the oxidation of $I^-$ on $KCa_2Nb_3O_{10}$, leading to $O_2$ evolution even in the presence of higher concentration of NaI.

### Effect of $Na^+$

As demonstrated above, the photocatalytic activity of Pt/$KCa_2Nb_3O_{10}$ restacked nanosheets for overall water splitting was promoted in the presence of $Na^+$ as well. In order to elucidate the reason, the reacted Pt/$KCa_2Nb_3O_{10}$ samples in the presence of various salts were characterized by XRD. Fig. 5 displays the X-ray diffraction peaks of Pt/$KCa_2Nb_3O_{10}$ attributed to the (002) plane, which is the stacking direction of restacked nanosheets. The diffraction peaks were shifted to lower two-theta directions after photocatalytic reactions in all cases, indicating that the (002) plane distance, namely the interlayer distance of restacked nanosheets, was expanded most likely due to an intercalation of water in the interlayer space, as reported previously.[6] It should be noted that the peak positions were altered depending on the cations in the reaction solution. Pt/$KCa_2Nb_3O_{10}$ after photocatalytic reaction in the presence of $Na^+$ exhibited 002 diffraction peaks at lower two-theta positions compared to the peaks

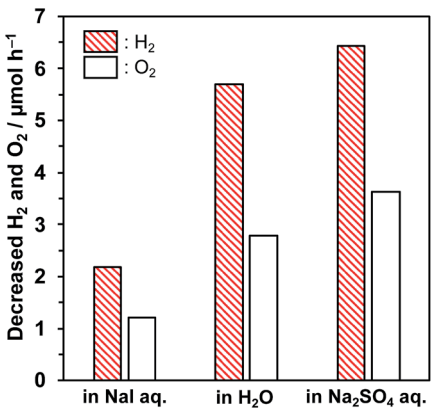


Fig. 3 Decreasing rates of $H_2$ and $O_2$ evolution over Pt/$KCa_2Nb_3O_{10}$ in aqueous NaI solution (10 mM), pure water, and $Na_2SO_4$ solution (5 mM) under dark conditions. Reaction conditions: photocatalyst, 50 mg; reactant volume, 100 mL; introduced amount of $H_2$, *ca.* 200 μmol and $O_2$, *ca.* 100 μmol.

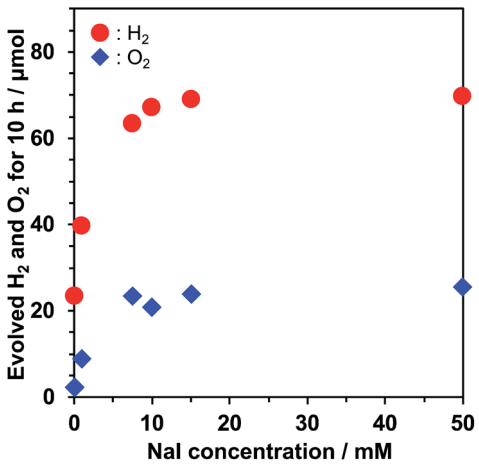


Fig. 4 Dependence of the photocatalytic water splitting activity of Pt/$KCa_2Nb_3O_{10}$ on the NaI concentration. Reaction conditions: catalyst, 50 mg; reaction solution, 100 mL; light source, a 300 W Xe lamp ($\lambda \geq$ 300 nm).

Open Access Article. Published on 03 Desember 2018. Downloaded on 15/03/2026 14.09.46.
This article is licensed under a Creative Commons Attribution-NonCommercial 3.0 Unported Licence.

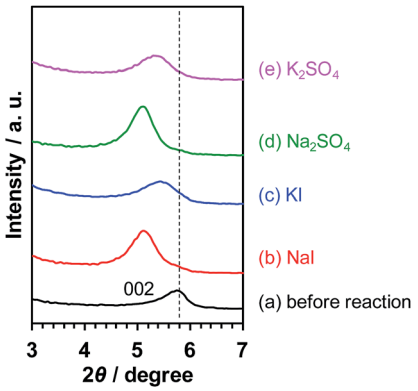


Fig. 5 002 diffraction peaks of Pt/$KCa_2Nb_3O_{10}$ in XRD (a) before reaction and after reaction in aqueous (b) NaI (10 mM), (c) KI (10 mM), (d) $Na_2SO_4$ (5 mM), and (e) $K_2SO_4$ (5 mM) solution.

in the presence of $K^+$, suggesting that a structural change occurred during the water splitting reaction.

It is known that interlayer cations of certain layered materials can be exchanged for $H^+$ and/or other kinds of alkali cations.[42] Therefore, one possibility is that the $K^+$ in the interlayer space of Pt/$KCa_2Nb_3O_{10}$ was exchanged for $Na^+$, which was present in the reaction solution. As shown in Fig. 6, XPS analysis revealed that photoelectron signals attributable to the K 2p orbital almost disappeared, while new peaks corresponding to the Na 1s orbital were clearly detected after reactions in aqueous NaI and $Na_2SO_4$ solution. In contrast, photoelectron singles of not Na 1s, but K 2p were observed before and after reaction in aqueous KI and $K_2SO_4$ solution. The results indicate that the ion-exchange of $K^+$ in the interlayer for $Na^+$ occurred, and that the structure of Pt/$KCa_2Nb_3O_{10}$ restacked nanosheets after reaction turned into Pt/$NaCa_2Nb_3O_{10}$.

The ion-exchange, however, does not seem to explain the shift of the diffraction peak position (Fig. 5). The ionic radius of $Na^+$ (1.02 Å) in a 6-coordination environment is smaller than that of $K^+$ (1.38 Å). Thus, one can suppose that the 002 diffraction peak after ion-exchange of $K^+$ for $Na^+$ appears at a higher two-theta position because of the smaller size of $Na^+$ and the resulting shorter (002) plane distance. A plausible

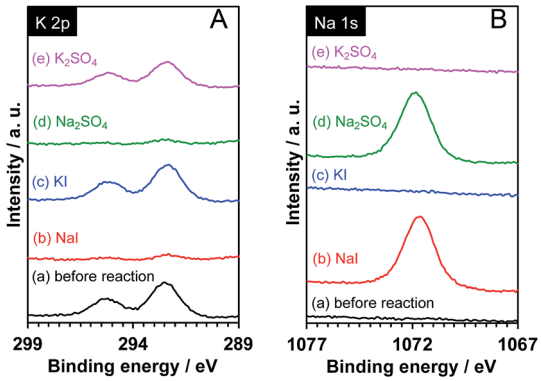


Fig. 6 XPS spectra for (A) K 2p and (B) Na 1s of Pt/$KCa_2Nb_3O_{10}$ (a) before and after reaction in aqueous (b) NaI (10 mM), (c) KI (10 mM), (d) $Na_2SO_4$ (5 mM), and (e) $K_2SO_4$ (5 mM) solution.

Table 2 Specific surface area of $KCa_2Nb_3O_{10}$ and $NaCa_2Nb_3O_{10}$ restacked nanosheets estimated from $N_2$ and $H_2O$ adsorption

| Material | $S_{N_2}$/m$^2$ g$^{-1}$ | $S_{H_2O}$/m$^2$ g$^{-1}$ | $S_{H_2O}/S_{N_2}$ |
|---|---|---|---|
| $KCa_2Nb_3O_{10}$ | 10.7 | 30.2 | 2.8 |
| $NaCa_2Nb_3O_{10}$ | 10.0 | 48.3 | 4.8 |

explanation for the phenomena opposite to our expectation is more hydration of the interlayer of Pt/$NaCa_2Nb_3O_{10}$, concealing the effect of $K^+/Na^+$ exchange.

In order to evaluate the correlation between interlayer cations and the affinity for water, we measured $H_2O$ and $N_2$ adsorption isotherms of $KCa_2Nb_3O_{10}$ and $NaCa_2Nb_3O_{10}$ (Fig. S3†). The surface areas estimated from the $H_2O$ and $N_2$ isotherms (represented as $S_{H_2O}$ and $S_{N_2}$, respectively) are listed in Table 2. In both cases of $KCa_2Nb_3O_{10}$ and $NaCa_2Nb_3O_{10}$, the specific surface areas estimated from $H_2O$ adsorption ($S_{H_2O}$) were larger than those from $N_2$ adsorption ($S_{N_2}$), indicating that $H_2O$ molecules could penetrate into the interlayer space of these materials. Although $S_{N_2}$ was not affected by interlayer cations, $NaCa_2Nb_3O_{10}$ exhibited obviously larger $S_{H_2O}$ than $KCa_2Nb_3O_{10}$. It is thus likely that the stronger affinity for $H_2O$ promoted the photo-redox reaction in the interlayer space of $Na^+$-exchanged Pt/$KCa_2Nb_3O_{10}$, leading to higher photocatalytic performance for overall water splitting.

Ebina *et al.* suggested that $Na^+$ ions in the interlayer of restacked nanosheets have stronger affinity toward water than $K^+$.[6] Very recently, we also reported that a layered metal oxide photocatalyst, $K_2CaNaNb_3O_{10}$, provided better access for reactant(s) in the interlayer space, which led to higher photocatalytic performance.[43] Therefore, the enhanced photocatalytic activity in the presence of $Na^+$ is ascribed to better affinity for water in the interlayer of restacked nanosheets, which resulted from the ion-exchange reaction of $K^+$ to $Na^+$. Because interlayer modification is very important for enhancing the activity of nanosheet photocatalysts, we believe that the finding of this work would be an "indirect" means of decorating the interlayer nanospace of ion-exchangeable metal oxide nanosheets that improves photocatalytic activity for overall water splitting.

## Conclusions

Effects of co-existing ions on the photocatalytic water splitting activity of Pt nanocluster-intercalated $KCa_2Nb_3O_{10}$ restacked nanosheets were investigated. The performance was much improved in aqueous NaI solution, compared to the pure water case, in terms of gas evolution rate, stability and $H_2/O_2$ stoichiometry. The results strongly suggest that during the water splitting reaction, $I^-$ ions suppressed $H_2/O_2$ recombination and photo-reduction of $O_2$. Furthermore, $K^+$ ions in the interlayer of Pt/$KCa_2Nb_3O_{10}$ underwent ion-exchange for $Na^+$ in the $Na^+$-containing reaction solution, producing Pt/$NaCa_2Nb_3O_{10}$. $H_2O$ and $N_2$ adsorption measurements demonstrated that $NaCa_2Nb_3O_{10}$ had better affinity for $H_2O$ in the interlayer space than $KCa_2Nb_3O_{10}$. It appears that this character of $NaCa_2Nb_3O_{10}$ is the key to improving the accessibility of $H_2O$ and the photocatalytic redox reaction in the interlayer space.

Open Access Article. Published on 03 Desember 2018. Downloaded on 15/03/2026 14.09.46.
This article is licensed under a Creative Commons Attribution-NonCommercial 3.0 Unported Licence.

## Conflicts of interest

There are no conflicts to declare.

## Acknowledgements

This work was partially supported by a Grant-in-Aid for Scientific Research on Innovative Areas "Mixed Anion" (Project JP16H06441) from the Japan Society for the Promotion of Science (JSPS). T. O. wishes to acknowledge support by a JSPS Fellowship for Young Scientists (Project JP16J10084). The authors thank Prof. Masashi Hattori and Michikazu Hara (Tokyo Institute of Technology) for assistance in XPS measurements.

## Notes and references

1 A. Kudo and Y. Miseki, *Chem. Soc. Rev.*, 2009, **38**, 253–278.
2 K. Maeda, *J. Photochem. Photobiol., C*, 2011, **12**, 237–268.
3 Y. Wang, H. Suzuki, J. Xie, O. Tomita, D. J. Martin, M. Higashi, D. Kong, R. Abe and J. Tang, *Chem. Rev.*, 2018, **118**, 5201–5241.
4 R. E. Schaak and T. E. Mallouk, *Chem. Mater.*, 2000, **12**, 2513–2516.
5 Y. Ebina, T. Sasaki, M. Haruda and M. Watanabe, *Chem. Mater.*, 2002, **14**, 4390–4395.
6 Y. Ebina, N. Sakai and T. Sasaki, *J. Phys. Chem. B*, 2005, **109**, 17212–17216.
7 H. Hata, S. Kudo, Y. Kobayashi and T. E. Mallouk, *J. Am. Chem. Soc.*, 2007, **129**, 3064–3065.
8 S. Ida, C. Ogata, K. Izawa, T. Inoue, O. Altuntasoglu and Y. Matsumoto, *J. Am. Chem. Soc.*, 2007, **129**, 8956–8957.
9 H. Hata, Y. Kobayashi, V. Bojan, W. J. Youngblood and T. E. Mallouk, *Nano Lett.*, 2008, **8**, 794–799.
10 S. Ida, C. Ogata, M. Eguchi, W. J. Youngblood, T. E. Mallouk and Y. Matsumoto, *J. Am. Chem. Soc.*, 2008, **130**, 7052–7059.
11 R. Ma, Y. Kobayashi, W. J. Youngblood and T. E. Mallouk, *J. Mater. Chem.*, 2008, **18**, 5982–5985.
12 K. Maeda, M. Eguchi, W. J. Youngblood and T. E. Mallouk, *Chem. Mater.*, 2008, **20**, 6770–6778.
13 M. C. Sarahan, E. C. Carroll, M. Allen, D. S. Larsen, N. D. Browning and F. E. Osterloh, *J. Solid State Chem.*, 2008, **181**, 1678–1683.
14 K. Maeda, M. Eguchi, W. J. Youngblood and T. E. Mallouk, *Chem. Mater.*, 2009, **21**, 3611–3617.
15 K. Maeda and T. E. Mallouk, *J. Mater. Chem.*, 2009, **19**, 4813–4818.
16 M. R. Allen, A. Thibert, E. M. Sabio, N. D. Browning, D. S. Larsen and F. E. Osterloh, *Chem. Mater.*, 2010, **22**, 1220–1228.
17 E. M. Sabio, M. Chi, N. D. Browning and F. E. Osterloh, *Langmuir*, 2010, **26**, 7254–7261.
18 S. Ida and T. Ishihara, *J. Phys. Chem. Lett.*, 2014, **5**, 2533–2542.
19 S. Ida, A. Takashiba, S. Koga, H. Hagiwara and T. Ishihara, *J. Am. Chem. Soc.*, 2014, **136**, 1872–1878.
20 K. Maeda, M. Eguchi and T. Oshima, *Angew. Chem., Int. Ed.*, 2014, **53**, 13164–13168.
21 T. Oshima, O. Ishitani and K. Maeda, *Adv. Mater. Interfaces*, 2014, **1**, 1400131.
22 K. Maeda, G. Sahara, M. Eguchi and O. Ishitani, *ACS Catal.*, 2015, **5**, 1700–1707.
23 T. Oshima, D. Lu, O. Ishitani and K. Maeda, *Angew. Chem., Int. Ed.*, 2015, **54**, 2698–2702.
24 T. Oshima, M. Eguchi and K. Maeda, *ChemSusChem*, 2016, **9**, 396–402.
25 T. Oshima, D. Lu and K. Maeda, *ChemNanoMat*, 2016, **2**, 748–755.
26 Y. Xia, W. Chen, S. Liang, J. Bi, L. Wu and X. Wang, *Catal. Sci. Technol.*, 2017, **7**, 5662–5669.
27 Y. Xia, S. Liang, L. Wu and X. Wang, *Catal. Today*, 2018, DOI: 10.1016/j.cattod.2018.03.061.
28 F. Amano, A. Yamakata, K. Nogami, M. Osawa and B. Ohtani, *J. Am. Chem. Soc.*, 2008, **130**, 17650–17651.
29 A. Kudo, A. Tanaka, K. Domen and T. Onishi, *J. Catal.*, 1988, **111**, 296–301.
30 K. Maeda and T. E. Mallouk, *Bull. Chem. Soc. Jpn.*, 2018, DOI: 10.1246/bcsj.20180258.
31 K. Sayama and H. Arakawa, *J. Chem. Soc., Faraday Trans.*, 1997, **93**, 1647–1654.
32 R. Abe, K. Sayama and H. Arakawa, *Chem. Phys. Lett.*, 2003, **371**, 360–364.
33 R. Abe, K. Sayama and H. Sugihara, *J. Phys. Chem. B*, 2005, **109**, 16052–16061.
34 H. Kato, Y. Sasaki, A. Iwase and A. Kudo, *Bull. Chem. Soc. Jpn.*, 2007, **80**, 2457–2464.
35 K. Maeda, H. Masuda and K. Domen, *Catal. Today*, 2009, **147**, 173–178.
36 Y. Miseki, H. Kusama, H. Sugihara and K. Sayama, *Chem. Lett.*, 2010, **39**, 846–847.
37 H. Suzuki, O. Tomita, M. Higashi and R. Abe, *J. Mater. Chem. A*, 2017, **5**, 10280–10288.
38 R. Abe, M. Higashi and K. Domen, *ChemSusChem*, 2011, **4**, 228–237.
39 M. Higashi, R. Abe, K. Teramura, T. Takata, B. Ohtani and K. Domen, *Chem. Phys. Lett.*, 2008, **452**, 120–123.
40 K. Maeda, M. Higashi, D. Lu, R. Abe and K. Domen, *J. Am. Chem. Soc.*, 2010, **132**, 5858–5868.
41 K. Maeda, D. Lu and K. Domen, *ACS Catal.*, 2013, **3**, 1026–1033.
42 M. Machida, T. Mitsuyama, K. Ikeue, S. Matsushima and M. Arai, *J. Phys. Chem. B*, 2005, **109**, 7801–7806.
43 T. Oshima, T. Yokoi, M. Eguchi and K. Maeda, *Dalton Trans.*, 2017, **46**, 10594–10601.

 This journal is © The Royal Society of Chemistry 2019